Modeling Colloid Attachment, Straining, and Exclusion in Saturated Porous Media

SCOTT A. BRADFORD,* JIRKA SIMUNEK,
MEHDI BETTAHAR,
MARTINUS TH. VAN GENUCHTEN, AND
SCOTT R. YATES

*George E. Brown, Jr., Salinity Laboratory, USDA, ARS,
450 West Big Springs Road, Riverside, California 92507-4617*

A conceptual model for colloid transport is developed that accounts for colloid attachment, straining, and exclusion. Colloid attachment and detachment is modeled using first-order rate expressions, whereas straining is described using an irreversible first-order straining term that is depth dependent. Exclusion is modeled by adjusting transport parameters for colloid-accessible pore space. Fitting attachment and detachment model parameters to colloid transport data provided a reasonable description of effluent concentration curves, but the spatial distribution of retained colloids at the column inlet was severely underestimated for systems that exhibited significant colloid mass removal. A more physically realistic description of the colloid transport data was obtained by simulating both colloid attachment and straining. Fitted straining coefficients were found to systematically increase with increasing colloid size and decreasing median grain size. A correlation was developed to predict the straining coefficient from colloid and porous medium information. Numerical experiments indicated that increasing the colloid excluded volume of the pore space resulted in earlier breakthrough and higher peak effluent concentrations as a result of higher pore water velocities and lower residence times, respectively. Velocity enhancement due to colloid exclusion was predicted to increase with increasing exclusion volume and increasing soil gradation.

Introduction

Knowledge of colloid transport and fate is required to assess contamination potential and to protect drinking water supplies from pathogenic microorganisms (*1*), to develop engineered bioaugmentation and bioremediation strategies (*2*), to microbially enhance oil recovery (*3*), and to quantify colloid-facilitated transport of many organic and inorganic contaminants (*4*). Colloid transport theory has been derived from a combination of convection-dispersion-retardation theory for solute transport and colloid attachment theory (*5, 6*). Traditional attachment theory employs irreversible first-order kinetic attachment of colloids (*7*) that predicts an exponential decrease in colloid concentration with distance in porous media. Complex correlations have been developed between experimental attachment coefficients and various physical and chemical variables (*8, 9*). These correlations predict an optimum particle size for transport for a given aqueous–porous medium system (*10*). Smaller particles are predicted to be removed more efficiently by diffusive transport and larger particles by sedimentation and interception.

A constant first-order attachment rate coefficient is typically used to describe colloid transport under initial or clean-bed conditions and when the fractional surface coverage of the porous media is small. Studies investigating the transport of microorganisms, however, have shown that the spatial distribution of retained microorganisms is not always consistent with a unique value of the attachment coefficient (*11–16*). Furthermore, attachment coefficients are reported to increase due to filter ripening (*17–19*) or decrease due to filling of favorable attachment sites (*20–22*). Predicted attachment coefficients have also been found to be underestimated when repulsive forces exist between the colloids and porous media (*12, 23*). Previous studies suggest that soil surface roughness (*24, 25*), charge heterogeneity (*21*), and variability in colloid characteristics (*26*) may be responsible for these discrepancies.

Some of the discrepancies between colloid transport data and attachment theory may also be due to the fact that colloid attachment theory does not account for straining. Straining is the trapping of colloid particles in down-gradient pore throats that are too small to allow particle passage (*6*). The magnitude of colloid retention by straining depends on both colloid and porous medium properties. Straining occurs when colloids are retained in pores that are smaller than some critical size. Colloid transport may still occur in pores that are larger than this critical size. Few studies have examined the influence of soil pore size distribution characteristics on colloid straining. Sakthivadivel (*27, 28*) and Herzig et al. (*29*) developed geometric relations between the effective diameter of colloids and soil grain size distribution characteristics to predict mass removal by straining. Matthess and Pekdeger (*30*) generalized this rule to porous media made up of a distribution of grain sizes. Bradford et al. (*31*) suggested that measured capillary pressure curves and residual saturations can also be used to provide an estimate of the volume fraction of the pore space that has pores less than some critical pore diameter for straining.

Colloid transport data from Harvey et al. (*32*) and Bradford et al. (*31*) indicate that straining was more pronounced than predictions based upon the criteria given by Matthess and Pekdeger (*30*). Harvey et al. (*32*) observed increasing colloid retention with increasing colloid size and hypothesized that migration of clay particles was responsible for this straining behavior. Bradford et al. (*31*) reported that effluent colloid concentration curves and the final spatial distribution of colloids retained by the porous media is highly dependent on the colloid size and soil grain size distribution. Relative peak effluent concentrations decreased, and the mass of colloids retained at the column inlet increased when the colloid size increased and the soil median grain size decreased. These observations were attributed to increased straining of the colloids. Bradford et al. (*31*) also examined the experimental colloid transport data using a traditional first-order attachment and detachment model. The observed removal trends were not consistent with traditional attachment theory. In contrast to the criteria given by Matthess and Pekdeger (*30*), the reported residual saturation values for the experimental soils employed by Bradford et al. (*31*) indicate that 2–30% of the pore space contain small pores (less than 10 μm) that may have contributed to the observed straining behavior. We are unaware of any models that explicitly account for colloid straining.

* Corresponding author phone: (909)369-4857; fax: (909)342-4963; e-mail: sbradford@ussl.ars.usda.gov.

A conceptual model is presented herein to account for both colloid attachment and straining. Colloid attachment is described using traditional attachment theory, whereas colloid straining is quantified using an irreversible first-order straining factor that is depth dependent. The model also accounts for colloid exclusion (charge or size) by considering colloid accessible pore space and pore sizes. The ability of this model to describe the experimental colloid transport data of Bradford et al. (*31*) is tested and correlations for model parameters are developed. The calibrated model and correlations are then used to predict effluent concentration curves and the final spatial distribution of colloids in experimental systems.

Theory
The aqueous phase colloid mass balance equation is written herein as

$$\frac{\partial(\theta_w C)}{\partial t} = -\nabla \cdot J_T - E_{sw}^{att} - E_{sw}^{str} \tag{1}$$

where C [N L^{-3}; N and L denote number and length, respectively] is the colloid concentration in the aqueous phase, t [T] is time, θ_w [-] is the volumetric water content, J_T [N L^{-2} T^{-1}] is the total colloid flux (sum of the advective, dispersive, and diffusive fluxes), and E_{sw}^{att} [N L^{-3} T^{-1}] and E_{sw}^{str} [N L^{-3} T^{-1}] are the colloid mass transfer terms between the aqueous and solid phases due to colloid attachment and straining, respectively. In the absence of colloid inactivation or degradation, a generalized term for E_{sw}^{att} is given by

$$E_{sw}^{att} = \frac{\partial(\rho_b S_{att})}{\partial t} = \theta_w k_{att} \psi_{att} C - \rho_b k_{det} S_{att} \tag{2}$$

where ρ_b [M L^{-3}; M denotes mass] is the soil bulk density, S_{att} [N M^{-1}] is the solid-phase concentration of attached colloids, k_{att} [T^{-1}] is the first-order colloid attachment coefficient, k_{det} [T^{-1}] is the first-order colloid detachment coefficient, and ψ_{att} [-] is a dimensionless colloid attachment function. The value of ψ_{att} equals 1 for clean-bed conditions. Other functional forms for ψ_{att} have been proposed in the literature to account for colloid blocking, ripening, and nonexponential spatial distributions (*21, 25, 33*).

For the work reported in this manuscript we will employ traditional clean-bed colloid attachment theory by setting the value of ψ_{att} equal to one. In this case, colloid attachment theory can be incorporated into the k_{att} term as follows (*7*)

$$k_{att} = \frac{3(1 - \theta_w)}{2d_{50}} \eta \alpha \nu_w \tag{3}$$

where η [-] is the collector (porous medium) efficiency, α [-] is the colloid sticking efficiency, d_{50} [L] is the median porous medium grain diameter, and v_w [L T^{-1}] is the pore water velocity. The collector efficiency accounts for colloid removal due to diffusion, interception, and gravitational sedimentation (*7*). The value of η is frequently calculated using the following correlation written in terms of dimensionless variables (*7, 9*)

$$\eta = 4A_s^{1/3} N_{Pe}^{-2/3} + A_s N_{Lo}^{1/8} N_R^{15/8} + 0.00338 A_s N_G^{1.2} N_R^{-0.4} \tag{4}$$

where A_s [-] is the Happel correction factor, N_{Pe} [-] is the Peclet number, N_{Lo} [-] is London-van der Waals attractive forces number, N_R [-] is the interception number, and N_G [-] is the gravitational number. The value of α represents the fraction of particles colliding with the porous media that remain attached and therefore reflects the net effect of repulsive and attractive forces between colloids and solid surfaces. The value of α is usually derived from experimental breakthrough curves (*34, 35*) or from fitted values of k_{att} and calculated values of η (*36, 37*), although theoretical approaches have also been proposed to predict α (*35*).

Colloid attachment theory has been used to predict colloid transport behavior for a wide variety of colloid and porous media characteristics. Little attention has been payed to colloid and porous media parameter ranges that may limit applicability of the attachment model, because colloid straining has been assumed a priori to be insignificant (E_{sw}^{str} is set equal to 0 in eq 1). The following simple and flexible form for E_{sw}^{str} is utilized in our study to account for straining

$$E_{sw}^{str} = \frac{\partial(\rho_b S_{str})}{\partial t} = \theta_w k_{str} \psi_{str} C \tag{5}$$

where k_{str} [T^{-1}] is the straining coefficient, ψ_{str} [-] is a dimensionless colloid straining function, and S_{str} [N M^{-1}] is the solid-phase concentrations of strained colloids. The dependence of k_{str} on colloid and porous medium size will be demonstrated later in this manuscript.

Data from Bradford et al. (*31*) indicates that straining is a strong function of distance. A depth-dependent power law function for ψ_{str} will therefore be utilized

$$\psi_{str} = \left(\frac{d_{50} + z}{d_{50}}\right)^{-\beta} \tag{6}$$

where β [-] is a fitting parameter that controls the shape of the colloid spatial distribution, and z [L] is the down gradient distance from the porous medium inlet or some soil texture discontinuity in the medium. The value of d_{50} is used here as a surrogate parameter for pore length, while the quantity $(d_{50}+z)/d_{50}$ is related to the number of pore lengths. Equations 5 and 6 assume that colloids are accessible to all soil pores at the column inlet or at interfaces of soil textural discontinuities (ψ_{str} equals 1 when $z = 0$). Straining near the column inlet will cause some pores to become dead-ends, thus restricting mobile colloids to only the larger continuous pore networks. The number of dead-end pores is hypothesized to decrease with increasing distance because size exclusion and/or limited transverse dispersivity tend to keep colloids within the larger networks (bypassing smaller pores). Hence, straining is greatest at the column inlet and then is expected to decrease with increasing distance. Additional pore-scale studies are planned to test this conceptual model of straining.

Size exclusion may influence the transport behavior of colloids by limiting the mobility of particles to the larger pores (*12, 38*). If the electrostatic forces between colloids and porous media are repulsive, then the colloid may also be excluded from locations adjacent to solid surfaces due to charge exclusion. Charge exclusion of many anions has been well documented (*39, 40*). In that case only a portion of the pore space will be accessible to mobile colloid particles. If colloids are excluded from the smaller pore spaces, then they will likely sample the more conductive ranges of the pore water velocity distribution, and hence be transported faster than a conservative solute tracer (*41–43*). To account for both size and charge exclusion behavior, values of θ_w and the Darcy water velocity, q_w [L T^{-1}], that occur in eqs 1–3 and 5 are replaced with the colloid-accessible volumetric water content, θ_{cw} [-], and Darcy water velocity, q_{cw} [L T^{-1}], respectively. The values of θ_{cw} and q_{cw} are defined here as

$$\theta_{cw} = \theta_w - \in\gamma \tag{7}$$

$$q_{cw} = \frac{q_w k_{rcw}}{k_{rw}} \tag{8}$$

where ϵ [-] is the porosity, γ [-] is the water saturation that is not accessible to mobile colloids, k_{rw} [-] is the water relative permeability, and k_{rcw} [-] is the colloid accessible water relative permeability. The ratio of q_{cw} and θ_{cw} yields the colloid accessible pore water velocity, v_{cw} [L T^{-1}]. The value of k_{rw} is typically determined from capillary pressure data using a pore size distribution model (44, 45). In analogy to this approach, we determine the value of k_{rcw} using the pore size distribution model of Burdine (44) by adjusting its limits of integration to reflect the accessible pore space to colloids as

$$k_{rcw}(S_w) = S_w^2 \frac{\int_\gamma^{S_w} R(x)^2 dx}{\int_0^1 R(x)^2 dx} \quad S_w > \gamma \quad (9)$$

where S_w [-] is the water saturation, R [L] is the pore size, and x [-] is a dummy saturation variable of integration. When S_w is less than γ then the value of k_{rcw} is set equal to zero. The value of γ can be theoretically related to a critical pore radius for exclusion using Laplace's equation of capillarity and a capillary pressure curve.

The proposed colloid transport model discussed above was implemented into the HYDRUS-1D computer code (46). HYDRUS-1D is a finite element model for simulating water, heat, and multiple reactive solute movement in one-dimensional variably saturated porous media. The program numerically solves the Richards equation for saturated-unsaturated water flow and Fickian based advection dispersion equations for heat and solute transport. The code is coupled to a nonlinear least squares optimization routine based upon the Marquardt−Levenberg algorithm (47) to facilitate the estimation of transport parameters from experimental data and comes with a graphical user interface to manage input data, nodal discretization and editing, parameter allocation, problem execution, and visualization of results.

Model Applications

This section examines the ability of the proposed colloid transport model to describe the experimental transport data of Bradford et al. (31). Four different sized fluorescent colloids (Interfacial Dynamics Company, Portland, OR 97224) were employed in this study, with diameters (d_p [L]) equal to 0.45, 1.0, 2.0, and 3.2 μm. These microspheres had carboxyl surface functional groups grafted onto latex particle surfaces by the manufacturer to create a negatively charged hydrophobic colloid surface with a particle density of 1.055 g cm^{-3} and an air−water contact angle of 115.2 degrees.

Aquifer material used for the soil column experiments consisted of various sieve sizes of Ottawa sand (99.8% quartz which is negatively charged at a neutral pH. U.S. Silica, Ottawa, IL 61350). The Ottawa sands will be designated herein, from coarser to finer, as 2030, 3550, MIX, and 70110. These porous media were selected to encompass a range in soil grain size distribution characteristics. Specific properties of the 2030, 3550, MIX, and 70110 sands, include median grain size of 0.74, 0.36, 0.24, and 0.15 millimeters and uniformity index of 1.21, 1.88, 3.06, and 2.25, respectively.

The aqueous phase chemistry of the tracer, resident, and eluant solutions utilized in the soil column experiments was chosen to create a stabilized monodispersed suspension with the selected colloids. The initial resident and eluant solutions consisted of 0.001 M NaCl with its pH buffered to 6.98 using NaHCO$_3$ (5×10^{-5} M). The colloid-conservative tracer solution consisted of 0.001 M NaBr with its pH buffered to 6.73 using NaHCO$_3$ (5×10^{-5} M) and the initial colloid concentration (C_i). The value of C_i was 4.24×10^{11}, 3.86×10^{10}, 4.85×10^9, and 1.18×10^9 particles per liter for the 0.45, 1.0, 2.0, and 3.2 μm colloids, respectively.

TABLE 1. Soil Column Properties (Column Length, L; Porosity, ϵ; and Darcy Water Velocity, q_w) and the Recovered Effluent (M_E), Soil (M_S), and the Total Colloid Mass Fraction (MB_T)

soil type	d_p (μm)	q_w (cm min^{-1})	ϵ	L (cm)	M_E	M_S	MB_T
2030	0.45	0.10	0.37	13.2	0.90	0.11	1.01
2030	1.00	0.10	0.38	13.4	0.83	0.08	0.91
2030	2.00	0.10	0.37	12.2	0.47	0.37	0.84
2030	3.20	0.10	0.36	13.1	0.44	0.64	1.08
3550	0.45	0.10	0.34	12.7	0.84	0.15	0.99
3550	1.00	0.10	0.34	12.7	0.87	0.10	0.97
3550	2.00	0.10	0.34	12.8	0.26	0.52	0.78
3550	3.20	0.10	0.34	12.8	0.34	0.73	1.07
MIX	0.45	0.10	0.33	12.4	0.96	0.22	1.18
MIX	1.00	0.11	0.33	12.5	0.84	0.18	1.02
MIX	2.00	0.11	0.34	12.7	0.12	0.97	1.09
MIX	3.20	0.11	0.34	12.5	0.12	1.25	1.37
70110	0.45	0.11	0.34	12.7	0.66	0.32	0.98
70110	1.00	0.11	0.34	12.7	0.46	0.43	0.89
70110	2.00	0.11	0.35	13.0	0.07	0.96	1.03
70110	3.20	0.11	0.36	13.0	0.03	0.88	0.91

We refer to Bradford et al. (31) and the Supporting Information for a detailed description of the experimental materials, protocols, and data analysis. In brief, the colloid-conservative tracer solution was pumped (Darcy velocity of $\sim$0.1 cm min^{-1}) upward through columns ($\sim$13 cm in length) packed with water saturated sand for approximately 75 min, after which a three-way valve was used to switch the pumped solution to the eluant for another 175 min. Colloid concentration in the column effluent and retained on the media were determined by fluorescence measurements. Table 1 summarizes relevant properties of the column experiments that we examined. To account for mass balance errors in the experimental data, the concentration of colloids retained in the soil is multiplied by one minus the colloid mass balance in the effluent divided by the colloid mass balance in the soil. This approach assumes that the colloid mass balance error is associated primarily with the solid phase.

Four different model formulations will be considered: M1 − attachment and detachment (i.e., eqs 1 and 2); M2 − straining (i.e., eqs 1, 5, and 6); M3 − attachment, detachment, and straining (i.e., eqs 1−6); and M4 − attachment, detachment, straining, and exclusion (eqs 1−9). Models M1 and M2 assume that colloid retention occurs exclusively by attachment or straining, respectively, whereas M3 and M4 assume that both colloid attachment and straining may occur. For models M3 and M4 the attachment coefficient is predicted from eqs 3 and 4 and a fixed value of α. The value of α was determined from transport experiments conducted using the same porous medium and 0.45 μm carboxyl colloids; little or no straining occurs in these systems. The detachment rate coefficient used for M3 and M4 was obtained by fitting the colloid effluent concentration curves. All models (M1, M2, M3, and M4) employed the same value of the colloid hydrodynamic dispersivity, λ_H [L], for a particular colloid-porous medium system. This λ_H value was obtained by fitting to the colloid effluent concentration data. Simulated transport behavior was obtained by fitting specific model parameters to the effluent concentration curves and the spatial distribution of retained colloids. Tables 2−4 summarize the values of the fitted M1, M2, and M3 model parameters, respectively. Statistical parameters for the goodness of fit are also included, such as the coefficient of linear regression (r^2) and the standard error (SE).

Model M1

Figure 1a presents the observed and M1 model effluent concentration curves (relative colloid effluent concentration, C/C_i, versus pore volume) for several representative colloid
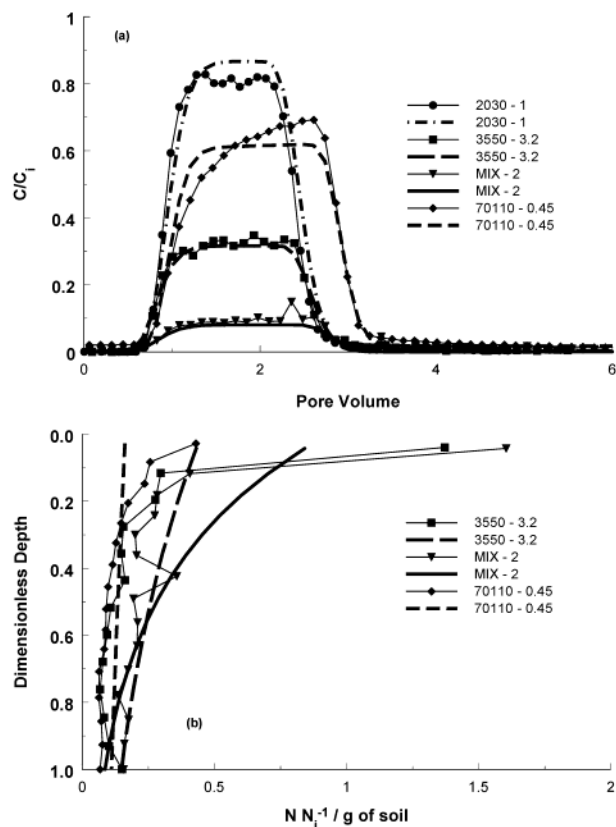
FIGURE 1. Observed and model M1 fitted effluent concentration curves (Figure 1a) and spatial distribution of retained colloids (Figure 1b) for several representative colloid transport experiments indicated in the legend. The first number in the legend indicates the soil type (cf. Table 1), and the second number is the colloid size in μm.
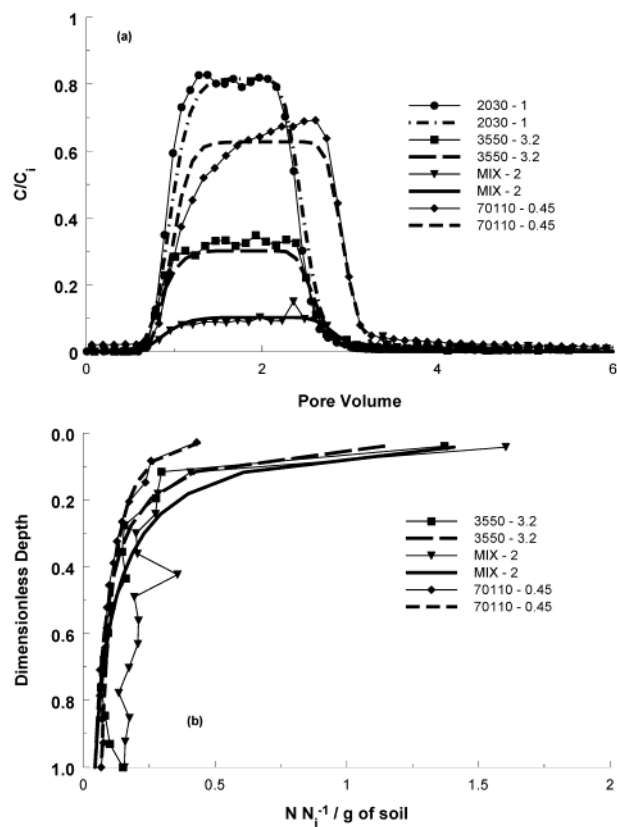

FIGURE 2. Observed and model M2 fitted effluent concentration curves (Figure 2a) and spatial distribution of retained colloids (Figure 2b) for several representative colloid transport experiments indicated in the legend.

transport experiments that encompass a range in transport behaviors. Notice that the M1 simulation fits describe the experimental data fairly well. Figure 1b presents the observed and M1 model normalized colloid number (N/N_i − number of colloids/initial number of colloids in effluent) per gram of dry soil as a function of normalized distance from the column inlet for several of the colloid transport experiments. The M1-simulated decrease in the colloid concentration with depth is generally much more gradual than that shown by the experimental data. This is especially true for systems in which significant colloid mass was retained at or near the soil surface. For example, compare the difference between M1 simulated and experimental 2 μm colloids in MIX sand with 0.45 μm colloids in 70110 sand. Although the effluent concentration curves in Figure 1a were adequately described using a fitted first-order attachment and detachment coefficient, Figure 1b suggests that this M1 modeling approach does not describe the observed spatial colloid distribution well for systems that exhibit significant colloid mass retention, presumably due to straining in these systems. For the model to be deemed "correct", both effluent and retention data must be simulated accurately.

Table 2 also presents calculated values of η according to eq 4. The value of η, for a particular soil type, is maximum for the smallest (0.45 μm) colloids and tends to achieve a minimum value for the 2.0 μm colloids. The attachment coefficients given in Table 2, however, tend to reach a maximum value for the largest colloids. To compensate for this deviation, values of α (as determined from eq 3 using the values of η and k_{att} given in Table 2) vary with colloid size and soil type. Recall that α theoretically accounts for the net effect of repulsive and attractive forces between colloids and solid surfaces. Since the electrostatic forces between the

various sized carboxyl colloids and Ottawa sands are similar in magnitude, the scatter in calculated values of α (2 orders of magnitude) reflects the inability of this approach to predict the experimental data. Ryan and Elimelech (12) also noted serious discrepancies between calculated sticking efficiencies and experimentally measured values. This limitation may occur in part because straining was not taken into account by attachment theory.

Other models that have been developed to describe time-dependent attachment behavior are not considered in the present study. It should be noted, however, that blocking implies that colloid retention decreases with increasing attached phase concentration and therefore produces less mass retention at the column inlet than clean-bed behavior. This is certainly not the case for our data. Conversely, ripening implies that colloid retention increases with increasing attached phase concentration and therefore produces more mass retention at the column inlet than clean-bed behavior. A second consequence of ripening is a decrease in colloid effluent concentration with increasing time of colloid addition. The experimental data examined in this manuscript do not support this second factor. In addition, the carboxyl colloids are strongly negatively charged and therefore exhibit a repulsive force between colloids that should inhibit ripening.

Model M2

Figure 2a shows observed and M2 model effluent concentration curves for several representative colloid transport experiments. Similar to the results in Figure 1, the M2 simulation describes the experimental effluent data fairly well. Figure 2b presents the observed and M2 model normalized colloid numbers per gram of dry soil as a function of normalized distance from the column inlet for several

TABLE 2. Fitted (k_{att} and k_{det} Were Fitted to Effluent and Retention Data) and Calculated (η — from Eq 4; and α — from Eq 3) M1 Model Parameters

soil type	d_p (μm)	λ_H (mm)	$k_{att} \times 10^3$ (min^{-1})	$SE \times 10^3$ (k_{att})	$k_{det} \times 10^3$ (min^{-1})	$SE \times 10^3$ (k_{det})	$\eta \times 10^2$	$\alpha \times 10^2$	r^2
2030	0.45	1.9	3.7	0.1	2.9	0.4	2.9	3.6	1.00
2030	1.00	2.4	2.9	0.5	0.0	1.7	1.8	4.6	0.94
2030	2.00	1.1	20.1	0.6	0.9	0.3	1.8	29.8	0.94
2030	3.20	2.4	19.3	0.6	0.4	0.2	2.9	17.6	0.94
3550	0.45	1.5	5.5	0.2	1.9	0.4	4.8	1.4	0.99
3550	1.00	1.6	3.6	0.1	0.6	0.4	3.0	1.5	1.00
3550	2.00	4.9	37.2	1.0	0.5	0.4	2.6	17.6	0.83
3550	3.20	2.9	30.2	3.1	0.0	0.4	3.5	10.6	0.58
MIX	0.45	1.0	3.4	0.2	6.9	0.9	6.3	0.4	1.00
MIX	1.00	1.8	5.6	0.3	1.3	0.4	3.9	1.1	0.99
MIX	2.00	3.9	67.1	12.5	0.0	0.9	3.1	16.7	0.66
MIX	3.20	3.6	72.0	10.9	0.0	1.0	4.0	13.4	0.74
70110	0.45	1.7	12.9	0.6	0.8	0.4	8.0	0.8	0.95
70110	1.00	0.7	22.4	1.1	0.6	0.4	5.2	2.1	0.86
70110	2.00	3.0	73.2	12.0	0.0	0.8	4.3	8.5	0.85
70110	3.20	3.6	101.5	62.4	0.1	3.4	5.1	9.9	0.67

TABLE 3. Fitted (k_{str} and β) M2 Model Parameters[a]

soil type	d_p (μm)	$k_{str} \times 10^3$ (min^{-1})	$SE \times 10^3$ (k_{str})	β	SE (β)	$RMSE$	r^2
2030	0.45	4.4	2.5	0.08	0.13	0.0	1.00
2030	1.00	4.1	0.8	0.00	0.05	7.1	0.95
2030	2.00	44.6	7.0	0.21	0.04	48.5	0.96
2030	3.20	33.1	5.0	0.14	0.04	8.0	0.95
3550	0.45	36.5	12.9	0.43	0.08	90.2	1.00
3550	1.00	18.9	5.3	0.36	0.06	83.3	1.00
3550	2.00	94.8	21.6	0.21	0.04	30.8	0.87
3550	3.20	906.8	185.1	0.78	0.05	91.5	0.97
MIX	0.45	9.2	7.8	0.34	0.20	0.0	0.99
MIX	1.00	21.3	14.1	0.28	0.13	0.0	0.99
MIX	2.00	989.4	149.9	0.57	0.04	77.1	0.93
MIX	3.20	427.5	58.5	0.44	0.06	54.6	0.89
70110	0.45	115.5	23.1	0.42	0.04	97.5	0.98
70110	1.00	271.9	146.1	0.47	0.11	69.0	0.94
70110	2.00	338.0	59.9	0.31	0.04	59.8	0.93
70110	3.20	2160.2	433.6	0.55	0.03	79.3	0.94

[a] The same value of λ_H that is given in Table 2 was employed in M2 simulation.

colloid transport experiments. The observed spatial distribution of colloids is more consistent with this model as compared to the M1 (Figure 1b) simulations. The reduction in error associated with the observed and (M2 compared to M1) simulated colloid spatial distributions is quantified in Table 3 using the relative mean square error (*RMSE*). *RMSE* is defined as the percentage of the difference in the colloid spatial distribution mean square error (*MSE*) of M1 and M2 divided by the *MSE* of M1. Hence, the *RMSE* values in Table 3 indicate that M2 exhibited a significant reduction in the simulated colloid spatial distribution error as compared to M1 (as much as 97%). Although M2 does a good job of describing both the effluent concentration curves and the final spatial distribution of colloids, it is unlikely that straining is the exclusive mechanism controlling mass removal. Batch and soil column experiments suggest that colloid attachment may also play a role (*31*). Hence, the improved description may be attributed in part to the increased flexibility (i.e., more adjustable parameters) of the M2 model.

Model M3

Figure 3a presents the observed and M3 model effluent concentration curves for several representative colloid transport experiments. Similar to the M1 and M2 simulations, notice that the M3 simulations describe the effluent data well. Figure 3b presents the observed and M3 model normalized colloid number per gram of dry soil as a function
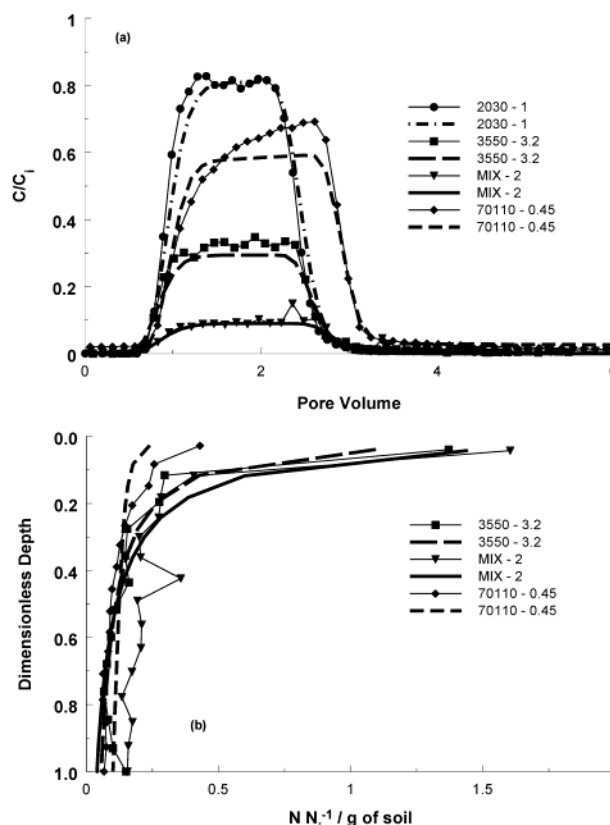
FIGURE 3. Observed and model M3 fitted effluent concentration curves (Figure 3a) and spatial distribution of retained colloids (Figure 3b) for several representative colloid transport experiments indicated in the legend. In this case, attachment was predicted using eqs 2–4 with the sticking efficiency determined from the 0.45 μm colloid transport experiment in a particular porous medium and straining parameters (β and k_{str}) were fitted to the data.

of normalized distance from the column inlet for several of these colloid transport experiments. The observed spatial distribution of colloids is accurately described by accounting for both colloid attachment and straining. Fitted and predicted M3 model parameters are given in Table 4, along with the percentage of total colloid mass retention via straining. The reduction in error associated with the observed and (M3 compared to M1) simulated colloid spatial distributions is quantified as before with *RMSE* values. The *RMSE* values in Tables 3 and 4 are quite similar, indicating that M3 also exhibited a significant reduction in the simulated

soil type	d_p (μm)	$k_{att} \times 10^3$ (min^{-1})	$k_{det} \times 10^3$ (min^{-1})	$k_{str} \times 10^3$ (min^{-1})	$SE \times 10^3$ (k_{str})	β	SE (β)	%MR_{str}	$RMSE$	r^2
2030	0.45	3.8	3.0	0.0	0.0	0.00	290.47	0.0	0.0	1.00
2030	1.00	2.3	0.1	2.0	0.5	0.00	0.05	46.9	7.7	0.95
2030	2.00	2.4	1.1	44.6	7.4	0.25	0.04	89.8	52.4	0.96
2030	3.20	4.0	0.4	31.7	5.6	0.18	0.04	80.9	9.7	0.95
3550	0.45	5.5	2.2	9.8	61.6	0.85	1.50	8.6	18.3	1.00
3550	1.00	3.4	0.7	28.0	47.2	1.00	0.65	18.6	60.6	1.00
3550	2.00	3.0	0.9	96.2	22.9	0.23	0.04	93.4	32.0	0.88
3550	3.20	4.1	0.3	814.1	208.5	0.78	0.06	92.3	89.5	0.97
MIX	0.45	3.1	4.5	5.4	38.0	1.00	2.17	7.5	0.0	1.00
MIX	1.00	1.9	1.0	83.0	57.6	0.68	0.19	71.5	28.8	0.99
MIX	2.00	1.5	0.6	1152.4	220.4	0.60	0.04	98.9	77.6	0.93
MIX	3.20	2.0	0.4	795.5	165.0	0.50	0.04	98.4	80.1	0.96
70110	0.45	12.7	1.4	76.2	110.8	0.76	0.42	20.0	44.1	0.97
70110	1.00	8.0	1.2	301.1	208.1	0.57	0.15	75.7	52.6	0.93
70110	2.00	6.5	0.7	367.5	69.2	0.34	0.04	93.0	61.1	0.93
70110	3.20	7.7	2.4	1853.0	334.9	0.58	0.06	97.8	77.1	0.94

[a] The value of k_{det} comes from Bradford et al. (31).

soil type	d_p (μm)	$k_{att} \times 10^3$ (min^{-1})	$k_{det} \times 10^3$ (min^{-1})	$k_{str} \times 10^3$ (min^{-1})	$SE \times 10^3$ (k_{str})	β	$RMSE$	r^2
2030	0.45	3.8	3.0	0.1	65.8	0.43	10.3	1.00
2030	1.00	2.3	0.1	10.4	327.1	0.43	9.0	0.95
2030	2.00	2.4	1.1	87.3	564.1	0.43	23.3	0.95
2030	3.20	4.0	0.4	79.4	330.2	0.43	-18.8	0.94
3550	0.45	5.5	2.2	1.4	82.6	0.43	13.3	0.99
3550	1.00	3.4	0.7	1.7	0.0	0.43	20.1	1.00
3550	2.00	3.0	0.9	242.7	2110.0	0.43	6.3	0.87
3550	3.20	4.1	0.3	220.5	575.4	0.43	72.0	0.88
MIX	0.45	3.1	4.5	2.2	0.0	0.43	0.0	1.00
MIX	1.00	1.9	1.0	29.3	78.4	0.43	25.6	0.99
MIX	2.00	1.5	0.6	560.1	411.4	0.43	73.8	0.91
MIX	3.20	2.0	0.4	632.4	274.1	0.43	82.5	0.95
70110	0.45	12.7	1.4	16.0	144.2	0.43	29.5	0.96
70110	1.00	8.0	1.2	153.4	303.0	0.43	57.3	0.92
70110	2.00	6.5	0.7	560.8	280.1	0.43	62.7	0.93
70110	3.20	7.7	2.4	1133.3	191.9	0.43	76.5	0.92

colloid spatial distribution error compared to M1 (as much as 90%).

Notice in Table 4 that the percentage of mass retention by straining (%MR_{str}) tends to increase with increasing colloid size. The percentage of mass retention via attachment follows from the mass balance. Hence, the percentage of mass retention by attachment decreases with increasing colloid size. For a given colloid size, the percentage of colloid mass retention by straining also tends to increase with decreasing soil median grain size. Although the percentage of mass retention by attachment is low for some of the total soil columns, as distance increases the relative importance of attachment increases in comparison to straining. For example, attachment accounted for 0.5 and 31.7% of the retained colloid mass at the column inlet and outlet, respectively, for the 3.2 μm colloids in 3550 sand. Eventually, colloid attachment may become the dominant mechanism for mass removal. Straining is believed to be diminished with increasing distance down gradient from the column inlet because size exclusion and/or limited transverse dispersivity tend to restrict colloids to the larger pore networks (bypassing smaller pores).

The M3 simulations shown in Figure 3a,b employ a different value of β for each colloid transport data set. Considering the shape similarity of the spatial distribution of retained colloids in systems that exhibit straining (cf. Figure 3b), we assume below that a single value of β may be employed to characterize straining behavior. For this purpose, the value of β was set equal to 0.43; i.e., the average β value

for the 2.0 and 3.2 μm colloids listed in Table 4. With this assumption, the value of k_{str} (M3 model) was again fitted to each colloid transport data set. Figure 4a,b shows the observed and M3 simulated fits to representative colloid transport data when β is set equal to 0.43. Notice in Figure 4a,b that the effluent concentration curves and the spatial distribution of retained colloids, respectively, are described well with the M3 model using $\beta = 0.43$. Table 5 presents the fitted values of k_{str} and the associated statistical parameters for the goodness of fit. The $RMSE$ values in Table 5 tend to be slightly lower than those given in Table 4 but still indicate a significant reduction in error when using M3 with fixed $\beta = 0.43$ compared to M1.

Figure 5 presents a plot of fitted k_{str} values (when $\beta = 0.43$) as a function of experimental d_p/d_{50} ratios. Notice that the value of k_{str} systematically increases with increasing d_p/d_{50}. This behavior is consistent with straining behavior; i.e., increasing with increasing colloid size and decreasing median grain size. The following power function correlation between k_{str} and d_p/d_{50} was established:

$$k_{str} = 269.7\left(\frac{d_p}{d_{50}}\right)^{1.42} \quad r^2 = 0.93 \quad (10)$$

The correlation prediction is shown in Figure 5 as a solid line. The above correlation, in conjunction with a fixed value of 0.43 for β and eqs 1, 5, and 6, now provides a first approximation to predict the influence of straining on colloid transport. We emphasize that straining will likely depend
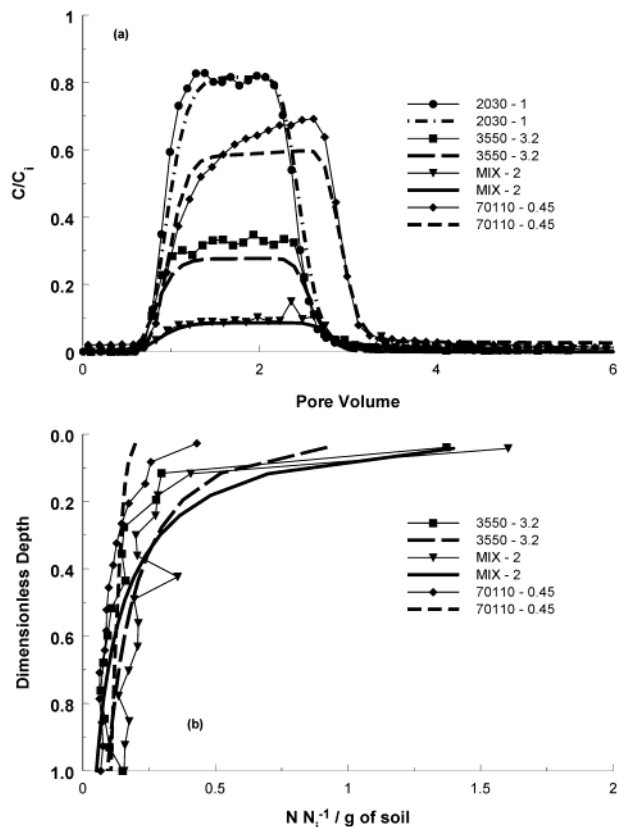
FIGURE 4. Observed and model M3 fitted effluent concentration curves (Figure 4a) and spatial distribution of retained colloids (Figure 4b) for several representative colloid transport experiments indicated in the legend. In this case, the attachment coefficient was predicted, a fixed value of $\beta = 0.43$ was employed (cf. eq 6), and only k_{str} was fitted to the data.
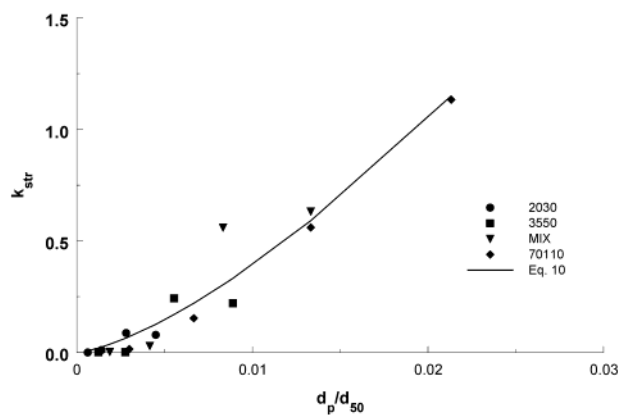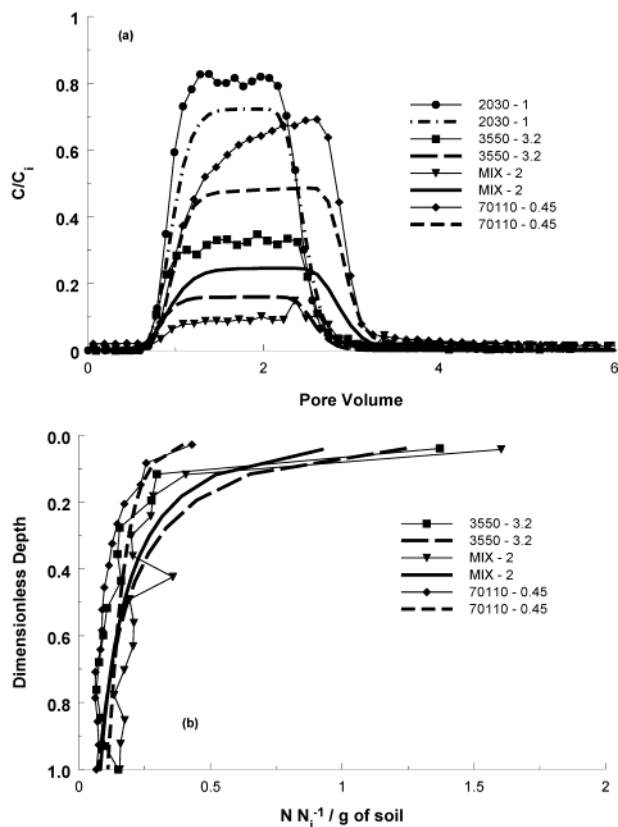
FIGURE 6. Observed and predicted M3 effluent concentration curves (Figure 6a) and spatial distribution of retained colloids (Figure 6b) for several representative colloid transport experiments indicated in the legend. Here straining behavior was predicted using eqs 5 and 6 with β set equal to 0.43 and k_{str} determined from eq 10. Attachment was predicted using eqs 2–4 with the sticking efficiency determined from the 0.45 μm colloid transport experiment in a particular porous medium.

FIGURE 5. A plot of fitted straining coefficient (k_{str}) values when $\beta = 0.43$ as a function of experimental d_p/d_{50} ratios (colloid diameter/ median grain size diameter).

also on other factors that are currently not included in the correlation, such as soil grain size uniformity, aqueous phase velocity, initial colloid concentration, colloid distribution, water content, experimental scale, colloid surface charge, aqueous phase chemistry, and solid-phase mineralogy. Additional experimental studies are needed to assess the influence of these factors on straining.

Figure 6a,b presents the observed and predicted effluent concentration curves and spatial distributions of retained colloids, respectively, for several representative colloid transport experiments. Here straining behavior was predicted using eqs 5 and 6 with β set equal to 0.43 and k_{str} determined from eq 10. Attachment was predicted using eqs 2–4 with

TABLE 6. Predicted (k_{att} and k_{str}) M3 Model Parameters

soil type	d_p (μm)	$k_{att} \times 10^3$ (min^{-1})	$k_{det} \times 10^3$ (min^{-1})	$k_{str} \times 10^3$ (min^{-1})	β	r^2
2030	0.45	3.8	3.0	7.9	0.43	1.00
2030	1.00	2.3	0.1	24.4	0.43	0.94
2030	2.00	2.4	1.1	65.2	0.43	0.95
2030	3.20	4.0	0.4	126.9	0.43	0.75
3550	0.45	5.5	2.2	20.6	0.43	0.99
3550	1.00	3.4	0.7	63.9	0.43	0.95
3550	2.00	3.0	0.9	170.8	0.43	0.77
3550	3.20	4.1	0.3	332.5	0.43	0.78
MIX	0.45	3.1	4.5	36.6	0.43	0.98
MIX	1.00	1.9	1.0	113.5	0.43	0.92
MIX	2.00	1.5	0.6	303.5	0.43	0.72
MIX	3.20	2.0	0.4	591.0	0.43	0.95
70110	0.45	12.7	1.4	71.3	0.43	0.95
70110	1.00	8.0	1.2	221.1	0.43	0.93
70110	2.00	6.5	0.7	591.0	0.43	0.93
70110	3.20	7.7	2.4	1151.0	0.43	0.92

the sticking efficiency determined from the 0.45 μm colloid transport experiment in a particular porous medium. The agreement between observed and predicted colloid transport is not always satisfactory. The model predictions do, however, capture the general trends in the observed data, notably increasing colloid retention with increasing colloid size and decreasing median grain size. Table 6 summarizes the parameter values used in the predictions and the statistical parameters for the goodness of the model description.
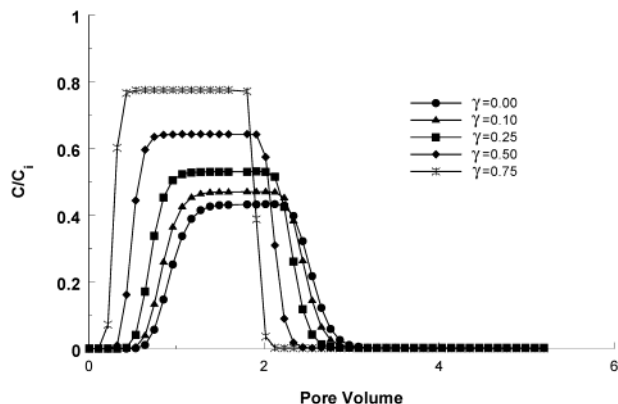
FIGURE 7. A plot of M4 simulated 3.2 μm colloid effluent concentration curves in 2030 sand for various values of γ (the water saturation that is not accessible to mobile colloids).
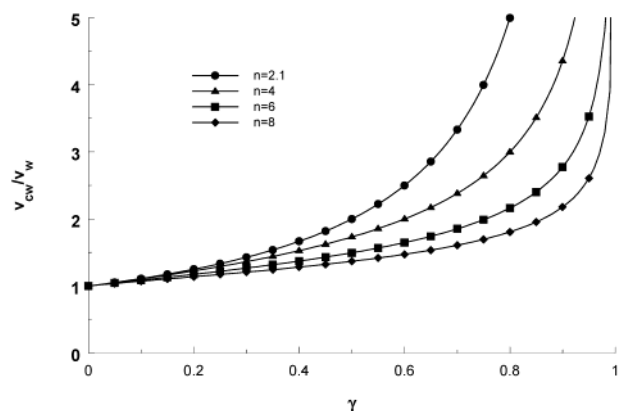

FIGURE 8. A plot of v_{cw}/v_w (colloid pore water velocity/average pore water velocity) as a function of γ for various hypothetical (saturated) porous media. The value of n in the figure legend corresponds to the van Genuchten (48) capillary pressure curve parameter ($m = 1-2/n$).

Model M4

The colloid transport data presented by Bradford et al. (31) did not exhibit earlier colloid breakthrough than bromide. Numerical experiments were therefore conducted to assess the sensitivity of model output to exclusion (charge and/or size). Figure 7 presents M4 simulated 3.2 μm colloid effluent concentration curves in 2030 sand (the relevant van Genuchten (48) capillary pressure curve parameters, are $n = 6.875$ with $m = 1-2/n$) for various values of γ. Notice that increasing γ leads to earlier colloid breakthrough and higher peak colloid concentrations as a result of an increase in the colloid pore water velocity and a decrease in the colloid residence time, respectively.

The predicted velocity enhancement (the ratio of the pore water velocity for colloids and a conservative solute, v_{cw}/v_w) for a particular porous medium as a function of γ can be easily calculated from eqs 7 and 8 and the analytical solution for eq 9 (49). The values of v_{cw}/v_w as a function of γ for various hypothetical (saturated) porous media are shown in Figure 8. The value of n in the figure legend corresponds to the van Genuchten (48) capillary pressure curve parameter ($m = 1-2/n$) and is related to the capillary pressure curve slope at the inflection point. A higher value of n corresponds to a more narrow pore size distribution. Hence, Figure 8 indicates that velocity enhancement is expected to increase in more graded soils and for larger values of γ. If the degree of velocity enhancement is known from experimental studies, then Figure 8 can also be used to estimate a value of γ. For example, Harter et al. (43) reported that *Cryptosporidium parvum*

oocysts (4.5−5.5 μm) were transported 1.19 and 1.37 times faster than chloride in coarse-textured sand, whereas Harvey et al. (50) reported that bacteria (0.5−0.7 μm) traveled 1.25 faster than bromide in a sandy glacial outwash aquifer. In these cases, Figure 8 implies that γ would range between 0.16 and 0.51 depending upon the porous medium type.

In general, smaller values of γ are probably more realistic since higher values of γ are also associated with greater colloid mass removal. Because the predicted velocity enhancement is less for smaller values of γ, greater travel distances may be required to accurately identify this exclusion phenomenon. Hence, larger-scale experiments may be better suited to investigate exclusion behavior than soil column studies.

Supporting Information Available

Additional information on materials and methods. This material is available free of charge via the Internet at http://pubs.acs.org.

Literature Cited

(1) Bitton, G.; Harvey, R. W. In *New Concepts in Environmental Microbiology*; Mitchell, R., Ed.; Wiley-Liss: New York, 1992; pp 103−124.
(2) Wilson, J. T.; Leach, L. E.; Henson, M.; Jones J. N. *Ground Water Monit. Rev.* **1986**, *6*, 56−64.
(3) MacLeod, F. A.; Lappin-Scott, H. M.; Costerton, J. W. *Appl. Environ. Microbiol.* **1998**, *54*, 1365−1372.
(4) Puls, R. W.; Powell, R. M. *Environ. Sci. Technol.* **1992**, *26*, 614−621.
(5) de Marsily, G. In *Quantitative hydrogeology: groundwater hydrology for engineers*; Academic Press: Orlando, FL, 1986.
(6) McDowell-Boyer, L. M.; Hunt, J. R.; Sitar, N. *Water Resour. Res.* **1986**, *22*, 1901−1921.
(7) Logan, B. E.; Jewett, D. G.; Arnold, R. G.; Bouwer, E. J.; O'Melia, C. R. *J. Environ. Eng.* **1995**, 121, 869−873.
(8) Yao, K.-M.; Habibian, M. T.; O'Melia, C. R. *Environ. Sci. Technol.* **1971**, *5*, 1105−1112.
(9) Rajagopalan, R.; Tien, C. *AIChE J.* **1976**, *22*, 523−533.
(10) Tobiason, J. E.; O'Melia, C. R. *J. Am. Water Works Assoc.* **1988**, *80*, 54−64.
(11) Swanton, S. W. *Adv. Colloid Interface Sci.* **1995**, *54*, 129−208.
(12) Ryan, J. N.; Elimelech, M. *Colloids and Surfaces A: Physicochem. and Eng. Aspects* **1996**, *107*, 1−56.
(13) Song, L. F.; Elimelech, M. *J. Colloid Interface Sci.* **1994**, *167*, 301−313.
(14) Song, L. F.; Johnson, P. R.; Elimelech, M. *Environ. Sci. Technol.* **1994**, *28*, 1164−1171.
(15) Bhattacharjee, S.; Ko, C.-H.; Elimelech, M. *Langmuir* **1998**, *14*, 3365−3375.
(16) Elimelech, M.; Nagai, M.; Ko, C. H.; Ryan, J. N. *Environ. Sci. Technol.* **2000**, *34*, 2143-2148.
(17) Tobiason, J. E. *Colloids Surfaces* **1989**, 39, 53−77.
(18) Darby, J. L.; Lawler, D. F. *Environ. Sci. Technol.* **1990**, *24*, 1069−1079.
(19) Tobiason, J. E.; Vigneswaran, B. *Water Res.* **1994**, 28, 335−342.
(20) Hunt, J. R.; Hwang, B.-C.; McDowell-Boyer, L. M. *Environ. Sci. Technol.* **1993**, *27*, 1099−1107.
(21) Johnson, P. R.; Elimelech, M. *Langmuir* **1995**, *11*, 801−812.
(22) Ko, C.-H.; Elimelech, M. *Environ. Sci. Technol.* **2000**, *34*, 3681−3689.
(23) Vaidyanathan, R.; Tien, C. *Chem. Eng. Sci.* **1991**, *46*, 967−983.
(24) Kretzschmar, R.; Barmettler, K.; Grolimund, D.; Yan, Y.-D.; Borkovec, M.; Sticher, H. *Water Resour. Res.* **1997**, *33*, 1129−1137.
(25) Redman, J. A.; Grant, S. B.; Olson, T. M.; Estes, M. K. *Environ. Sci. Technol.* **2001**, *35*, 1798−1805.
(26) Bolster, C. H.; Mills, A. L.; Hornberger, G. M.; Herman, J. S. *Water Resour. Res.* **1999**, *35*, 1797−1807.
(27) Sakthivadivel, R. *Theory and mechanism of filtration of non-colloidal fines through a porous medium*; Rep. HEL 15-5; Hydraulic Engineering Laboratory, University of California: Berkeley, CA 1966.
(28) Sakthivadivel, R., *Clogging of a granular porous medium by sediment*; Rep. HEL 15-7; Hydraulic Engineering Laboratory, University of California: Berkeley, CA, 1969.
(29) Herzig, J. P.; Leclerc, D. M.; LeGoff, P. *Ind. Eng. Chem.* **1970**, *62*, 129−157.

(30) Matthess, G.; A. Pekdeger, *Survival and transport of pathogenic bacteria and viruses in groundwater, in Ground Water Quality*; Ward, C. H., Giger, W., McCarty, P., Eds.; John Wiley: New York, 1985.

(31) Bradford, S. A.; Yates, S. R.; Bettahar, M.; Simunek, J. *Water Resour. Res.* **2002**, *38*(12), 1327, doi: 10.1029/2002WR001340.

(32) Harvey, R. W.; Kinner, N. E.; MacDonald, D.; Metge, D. W.; Bunn, A. *Water Resour. Res.* **1993**, *29*, 2713−2721.

(33) Adamczyk, Z.; Siwek, B.; Zembala, M.; Belouschek, P. *Adv. Colloid Interface Sci.* **1994**, *48*, 151−280.

(34) Pieper, A. P.; Ryan, J. N.; Harvey, R. W.; Amy, G. L.; Illangasekare, T. H.; Metge, D. W. *Environ. Sci. Technol.* **1997**, *31*, 1163−1170.

(35) Ryan, J. N.; Elimelech, M.; Ard, R. A.; Harvey, R. W.; Johnson, P. R. *Environ. Sci. Technol.* **1999**, *33*, 63−73.

(36) Bales, R. C.; Hinkle, S. R.; Kroeger, T. W.; Stocking, K. *Environ. Sci. Technol.* **1991**, *25*, 2088−2095.

(37) Redman, J. A.; Grant, S. B.; Olson, T. M.; Hardy, M. E.; Estes, M. K. *Environ. Sci. Technol.* **1997**, *31*, 3378−3383.

(38) Ginn, T. R. *Water Resour. Res.* **2002**, *38*(4), 1041, doi: 10.1029/2001WR000865.

(39) Gvirtzman, H.; Gorelick, S. M. *Nature* **1991**, *352*, 793−795.

(40) Ginn, T. R. *A brief review of bacterial transport in natural porous media*; PNL-10876; UC-402; Pacific Northwest National Laboratory: Richland, WA, 1995.

(41) Reimus, P. W. *The use of synthetic colloids in tracer transport experiments in saturated rock fractures*; LA-13004-T; Los Alamos National Laboratory: Los Alamos, NM, 1995.

(42) Cumbie, D. H.; McKay, L. D. *J. Contam. Hydrol.* **1999**, *37*, 139−157.

(43) Harter, T.; Wagner, S.; Atwill, E. R. *Environ. Sci. Technol.* **2000**, *34*, 62−70.

(44) Burdine, N. T. *Trans. Am. Inst. Min. Metall. Pet. Eng.* **1953**, *198*, 71−78.

(45) Mualem, Y. *Water Resour. Res.* **1976**, *12*, 513−522.

(46) Simunek, J.; Sejna, M.; van Genuchten, M. Th. *The HYDRUS-1D software package for simulating the one-dimensional movement of water, heat, and multiple solutes in variably saturated media − Version 2.0*; IGWMC − TPS − 70; International Ground Water Modeling Center, Colorado School of Mines: Golden, CO, 1998.

(47) Marquardt, D. W. *J. Soc. Indust. Appl. Math.* **1963**, *11*, 431−441.

(48) Van Genuchten, M. Th. *Soil Sci. Soc. Am. J.* **1980**, *44*, 892−898.

(49) Van Genuchten, M. Th.; Leij, F. J.; Yates, S. R. *The RETC code for quantying the hydraulic functions of unsaturated soils*; EPA/600/2-91/065; U.S. Environmental Protection Agency: Ada, OK, 1991.

(50) Harvey, R. W.; George, L. H.; Smith, R. L.; LeBlanc, D. R. *Environ. Sci. Technol.* **1989**, *23*, 51−56.